Mon. Not. R. Astron. Soc. **000**, 000–000 (0000) Printed 15 May 2014 (MN LATEX style file v2.2)

The High-z Universe Confronts Warm Dark Matter: Galaxy Counts, Reionization and the Nature of Dark Matter

Christian Schultz[1,2⋆], Jose Oñorbe[1], Kevork N. Abazajian[1], James S. Bullock[1]

[1]*Center for Cosmology, Department of Physics and Astronomy, 4129 Frederick Reines Hall, University of California, Irvine, CA 92697*
[2]*Department of Physics and Astronomy, Aarhus University, Ny Munkegade, DK-8000 Aarhus C, Denmark.*

15 May 2014

ABSTRACT

We use N-body simulations to show that high-redshift galaxy counts provide an interesting constraint on the nature of dark matter, specifically Warm Dark Matter (WDM), owing to the lack of early structure formation these models. Our simulations include three WDM models with thermal-production masses of 0.8 keV, 1.3 keV, and 2.6 keV, as well as CDM. Assuming a relationship between dark halo mass and galaxy luminosity that is set by the observed luminosity function at bright magnitudes, we find that 0.8 keV WDM is disfavored by direct galaxy counts in the Hubble Ultra Deep Field at $> 10\sigma$. Similarly, 1.3 keV WDM is statistically inconsistent at 2.2σ. Future observations with JWST (and possibly HST via the Frontier Fields) could rule out 1.3 keV WDM at high significance, and may be sensitive to WDM masses greater than 2.6 keV. We also examine the ability of galaxies in these WDM models to reionize the universe, and find that 0.8 keV and 1.3 keV WDM produce optical depths to the Cosmic Microwave Background (CMB) that are inconsistent at 68% C.L. with current Planck results, even with extremely high ionizing radiation escape fractions, and 2.6 keV WDM requires an optimistic escape fraction to yield an optical depth consistent with Planck data. Although CMB optical depth calculations are model dependent, we find a strong challenge for stellar processes alone to reionize the universe in a 0.8 keV and 1.3 keV WDM cosmology.

Key words: cosmology: Theory – cosmology: Halo mass function – cosmology: Abundance matching – cosmology: Reionization – galaxies: Luminosity function – cosmology: Dark matter

1 INTRODUCTION

Dark matter dominates the evolution of gravitational perturbations, leading to the formation of haloes and galaxies. In the prevalent paradigm of cold dark matter (CDM), the primordial perturbation spectrum extends to very small scales; galaxy formation proceeds from the bottom up, commencing in the smallest dark matter haloes where gas cooling can occur. If instead there exists a non-negligible minimal scale for primordial perturbations as in the case of warm dark matter (WDM), halo formation is delayed, and early galaxy formation is suppressed considerably.

Early galaxy formation has been understood to be a challenge for WDM models for some time (Barkana, Haiman & Ostriker 2001; Somerville, Bullock & Livio 2003). Today, the tension is only heightened by mounting evidence that structure formation is proceeding in earnest at very early cosmic times. There are now direct detections of galaxies at redshifts as high as $\sim$10 (Ellis et al. 2013; Oesch et al. 2013), clearly indicating that there are collapsed structures at this time. More indirectly, studies of quasar spectra show that the intergalactic medium was almost fully ionized by redshift $z \sim 6$ (Fan et al. 2006) and the measured electron scattering optical depth from the cosmic microwave background may could imply reionization as early as $z \sim 10$ (Ade et al. 2013). The maintenance of reionization back to these early times seems to require contributions from numerous, low-mass galaxies (Kistler et al. 2009; Kuhlen & Faucher-Giguere 2012; Robertson et al. 2013). In this paper, we examine how current and future observations of high-z galaxies, together with observational probes of reionization, can constrain the dark matter power spectrum on small scales, and by extension the particle nature of dark matter.

There has been considerable interest in the WDM paradigm for galaxy formation, owing to potential problems with the LCDM model on sub-galactic scales. Most recently, it has been recognized that the observed central densities of low-luminosity Milky Way dwarf satellite are significantly lower than expected in dissipationless CDM simulations (Boylan-Kolchin et al. 2012). This issue can be be alleviated if the dark matter is warm (Lovell et al. 2012, 2013; Polisensky & Ricotti 2013). Here, we specifically study a WDM

⋆ Email: cs06@phys.au.dk

model (1.3 keV thermal particle mass) that corresponds to the cut-off scale that alleviates the central-density problem. It should be noted here that models including ultra-light axions alongside a cold dark matter component can also alleviate the sub-galactic problems in the pure cold dark matter models (Marsh & Silk 2013).

The two most popular classes of WDM particle candidates are "thermal" particles and sterile neutrinos. Thermal WDM is coupled to the primordial plasma in the early Universe, and is diluted to the proper (observed) dark matter density by an unspecified process. Sterile neutrinos, on the other hand, can be produced at the proper dark matter abundance through scattering processes due to their mixing with active neutrinos with the Dodelson-Widrow mechanism (Dodelson & Widrow 1994, sometimes referred to as non-resonant production), through resonant production in the case of a large cosmological lepton asymmetry (Shi & Fuller 1999), or through coupling with other fields (Kusenko 2006; Shaposhnikov & Tkachev 2006). An important characteristic of the different models is the free streaming length they introduce, with a given particle mass having a different free-streaming length for the different WDM particles and for the different sterile neutrino production mechanisms. In this paper we primarily state particle masses in terms of thermal WDM particles, i.e., the "thermal mass", but we also provide conversions to the Dodelson-Widrow sterile neutrino mass in summary statements and tables. We also quote the wave numbers where the associated power spectra fall to half the value of a standard CDM model, which allows our results to be interpreted generally for any model that results in truncated small-scale power, as can arise for standard CDM particles in the case of non-standard inflation (e.g. Kamionkowski & Liddle 2000; Zentner & Bullock 2002).

Recent work has constrained the warm dark particle mass by a number of methods. Some of the currently tightest constraints come from observations of the Lyman-α (Lyα) forest produced by neutral gas along the line of sight to distant quasars. The neutral gas follows the gravitationally-dominant dark matter clustering in the mildly non-linear regime probed by the Lyα forest, and therefore it can be a powerful probe of the dark matter perturbation spectrum at small scales. However, the Lyα forest is a challenging tool, requiring disentangling the effects of pressure support and thermal broadening of the Lyα forest features from the effects of dark matter perturbation suppression from WDM. In addition, modeling the dependence on the physics of the neutral gas requires assumptions of the thermal history of the intergalactic medium and its ionizing background, which are done as parameterized fitting functions. Many of the limitations of the Lyα forest on constraints of the primordial power spectrum are discussed in Abazajian et al. (2011). Setting aside the limitations of the method, the Lyα forest provides stringent constraints, with recent quoted limits at $m_{\rm WDM} > 3.3$ keV (2σ, Viel et al. 2013).

The lack of early structure formation in WDM has motivated limits from the rate of high-z gamma-ray bursts (de Souza et al. 2013). Similarly, Pacucci et al. (2013) utilize strongly lensed ultra-faint, high redshift galaxies to constrain the particle mass by halo mass function considerations. At low redshift, WDM models can be constrained by studying the abundance of small galaxies. Work by Polisensky & Ricotti (2011) and Lovell et al. (2013) uses N-body simulations of Milky Way sized dark matter haloes and constrains the particle mass by assuming that the number of simulated dark matter satellites equals or exceeds the number of observed Milky Way satellites, and report limits on thermal WDM particle masses of $m_{\rm WDM} > 2.3$ keV and > 1.5 keV, respectively. It should be recognized that constraints from satellite counts are sensitive to halo-to-halo variation in substructure counts as well as assumed completeness corrections to the observed Milky Way satellite luminosity function. More recently, Horiuchi et al. (2013) have tried to adequately account for the halo-to-halo scatter and focused on counts around M31 (which are higher than around the MW at fixed luminosity) and find $m_{\rm WDM} > 1.8$ keV.

Given the potential systematic problems with known WDM constraints, it is useful to explore alternative probes. In the rapidly-evolving field of high-z galaxy surveys, the Lyman break technique has proven useful for discovering galaxies and estimating the UV luminosity function out to redshifts $z \sim 9$, although there are candidates in the literature at redshifts as high as $z \sim 12$ (Oesch et al. 2013; McLure et al. 2012; Bouwens et al. 2011; Schenker et al. 2013; Bouwens et al. 2007). New Fourier techniques seem promising in finding fainter candidates below the normally required detection threshold $S/N \sim 4.5$ (Calvi et al. 2013). Furthermore, Lyman break galaxies seem to be fair tracers of the overall halo population (Conroy et al. 2006). Thus the UV luminosity function interconnects with the halo mass function of dark matter, a quantity which is readily constructed from simulations and from which different dark matter models can be distinguished.

Additional physical mechanisms may ease the tension between simulations and observations presented by, e.g., the missing dwarf galaxies or the too-big-to-fail problem (Boylan-Kolchin et al. 2012). One example is the work Bovill & Ricotti (2011). Here it is noted that the Milky Way halo may be populated by fossils of early dwarf galaxies that formed before reionization, and that these fossils today have very low surface brightness rendering them outside of current observational bounds. Therefore, there may indeed be a population of low luminosity dwarf galaxies near the Milky Way. Katz & Ricotti (2012) expands on this result, and argues that the bulk of the old globular clusters in the Milky Way formed in these first (now fossil) dwarf galaxies. Furthermore, the proto-globular clusters were an important mode of star formation in these galaxies, and could in fact be the main driver for reionization.

In this work, we study in detail the effects of WDM models on high-z dark matter halo counts using high-resolution cosmological simulations, and extend these results empirically to infer the observable effects on galaxies and reionization. We compare the high-z luminosity functions of galaxies recently measured from the Hubble Ultra Deep Field (HUDF) with the inferred luminosity-function derived using N-body simulations in WDM and CDM cosmologies. Our predicted luminosity functions are normalized to match observed bright galaxy counts using abundance matching. All magnitudes quoted below are in the AB system. The same models allow us to study cosmological reionization in WDM models and compare them to CDM.

2 THEORY AND SIMULATIONS

2.1 Power Spectrum

WDM has a non-negligible thermal velocity which imprints a free streaming scale in the matter perturbation distribution arising from the early Universe. Below this free-streaming scale, structure formation is suppressed. This scale is conveniently parameterized by the Jeans mass

$$M_J(z) = \frac{4}{3\pi}\rho_{\rm dm}(z)\left(\frac{\pi\sigma_v^2(z)}{4G\bar{\rho}(z)}\right)^{3/2}, \qquad (1)$$

where $\rho_{\rm dm}$ is the dark matter density, $\bar{\rho}$ the mean density and σ_v the velocity dispersion. The Jeans mass is constant approximately

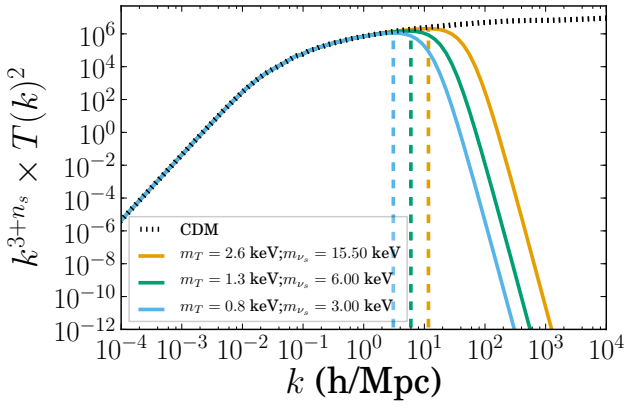

Figure 1. Shown are the matter power spectra for the different WDM models considered in this paper. The more massive the WDM particle, the more CDM-like the matter transfer function becomes due to the lower thermal velocities. For reference, each model is labeled by its equivalent thermal and sterile neutrino mass. The dashed lines mark the maximum of the transfer function.

until matter-radiation equivalence and thus erases the initial conditions below this mass scale. After matter-radiation equality the Jeans mass drops rapidly and decays with the cooling of the dark matter in the Hubble flow as $\sim a^{-3/2}$ (Schneider et al. 2013). The transfer function relates the primordial matter power spectrum to the linear power spectrum at a later redshift. For WDM, the matter power spectrum can be seen as a suppression of power above a certain wavenumber k. In fact, the transfer function for WDM relative to the CDM case can be approximated by the fitting function (Abazajian 2006):

$$T(k) = [1 + (\alpha k)^{\nu}]^{-\mu} \ , \tag{2}$$

where the smoothing scale is set by

$$\alpha = a \left(\frac{m_s}{\mathrm{keV}}\right)^{b} \left(\frac{\Omega_{\mathrm{dm}}}{0.26}\right)^{c} \left(\frac{h}{0.7}\right)^{d} h^{-1}\ \mathrm{Mpc}. \tag{3}$$

Here m_s is the (non-thermally produced) sterile neutrino WDM particle mass (Abazajian 2006). The relationship between the mass of a thermal particle (m_{WDM}) and the mass of the sterile neutrino (m_s) for which the transfer functions are nearly identical (Viel et al. 2005) is:

$$m_{\mathrm{WDM}} = 0.335\ \mathrm{keV} \left(\frac{m_s}{\mathrm{keV}}\right)^{3/4} \left(\frac{\Omega_m}{0.266}\right)^{1/4} \left(\frac{h}{0.71}\right)^{1/2}. \tag{4}$$

Fig. 1 shows the matter power spectrum for the three WDM models we explore in this paper (labeled by thermal mass and equivalent sterile mass) along with a CDM model for comparison. For comparison purposes, the scales where these WDM transfer functions equal half the CDM transfer function, $k_{1/2}$, are listed in Table 1, along with wave number of maximum power k_{max}.

2.2 Numerical Simulations

Our simulations were performed with the GADGET-2 code, in TreePM mode (Springel 2005). In order to generate the initial conditions (ICs), we have used the MUSIC code (Hahn & Abel 2011). The method uses an adaptive convolution of Gaussian white noise with a real-space transfer function kernel together with an adaptive multi-grid Poisson solver to generate displacements and velocities

m_T	m_{ν_s}	$k_{1/2}$ [h/Mpc]	k_{max} [h/Mpc]
2.6 keV	15.5 keV	21.4	2.62
1.3 keV	6.0 keV	9.47	1.28
0.8 keV	3.0 keV	5.24	0.764

Table 1. Warm dark matter models simulated in this paper. The first column gives the thermal WDM mass. This is the default model label we use throughout the work. The second column gives the equivalent sterile neutrino mass. The last two columns list the wave numbers where the transfer functions reach half the value of CDM and the wave numbers where the power spectrum is maximized, respectively.

following second-order Lagrangian perturbation theory. For more specific details on the MUSIC code, we refer the reader to (Hahn & Abel 2011). The CAMB (Lewis et al. 2000; Howlett et al. 2012) package was used to generate the CDM transfer functions used to generate the ICs for this cosmology. The WDM transfer functions were obtained from CDM using equations (2)-(3). Only the initial conditions were modified, and the thermal velocities of the WDM particles are not included in the simulations, since they have not been found to be significant in affecting WDM structure formation (Bode et al. 2001; Villaescusa-Navarro & Dalal 2011).

The cosmological parameters used were $h = 0.71$, $\Omega_m = 0.266$, $\Omega_\Lambda = 0.734$, $n_s = 0.963$ and $\sigma_8 = 0.801$. All simulations are 1024^3 particles in (50 Mpc/h)^3 boxes started at $z_{ini} = 125$. The implied particle mass is $m_p = 8.6 \times 10^6 h^{-1} M_\odot$. We employ three WDM models with thermal particle masses of 0.8 keV, 1.3 keV and 2.6 keV, which are equivalent to oscillation-produced Dodelson-Widrow sterile neutrino particle masses of 3 keV, 6 keV, and 15.5 keV. Note that the 1.3 keV (thermal; 6 keV sterile) case is equivalent in the structure formation cutoff scale of the M2L25 model of Boyarsky et al. (2009) & Lovell et al. (2012).

Three separate issues require special attention when running these simulations: 1) The dependence of the halo mass function at high redshift on the chosen starting redshift, z_{ini}; 2) Systematic errors induced by the finite volume of the simulation; and 3) Artificial haloes that emerge in WDM as a result of shot noise in regimes where the underlying power spectrum is suppressed. We discuss each of these issues in turn.

Concerning the initial redshift z_{ini}, recent advances in the techniques used for numerical calculation of perturbations, such as the second order Lagrangian Perturbation Theory (2LPT; see, for example Jenkins 2010), have improved the convergence of simulations using different z_{ini}. Several groups (e.g. Lukić et al. 2007; Prunet et al. 2008; Knebe et al. 2009; Jenkins 2010; Reed et al. 2013) have worked to quantify the effect of z_{ini} on the final results of cosmological simulations. These works stress the point that not using 2LPT algorithm leads to simulations that converge very slowly as the start redshift is increased. In order to reduce as much as possible any z_{ini} effect we have used the 2LPT algorithm incorporated in MUSIC (Hahn & Abel 2011) to generate all the initial conditions of our simulations. Additionally, all the simulations presented in this work use the same initial redshift ($z_{ini} = 125$). Therefore any systematic effects associated with starting redshift will be present in all cases and cancel when considering the ratios between the WDM and CDM halo mass functions.

Systematic errors from the finite volume of the simulation box can be divided into 3 categories: Shot noise, sampling variance, and lack of power from modes larger than the simulation box. Shot noise is especially important for the most massive haloes since only a few exists in the simulation volume, and it generally decreases as

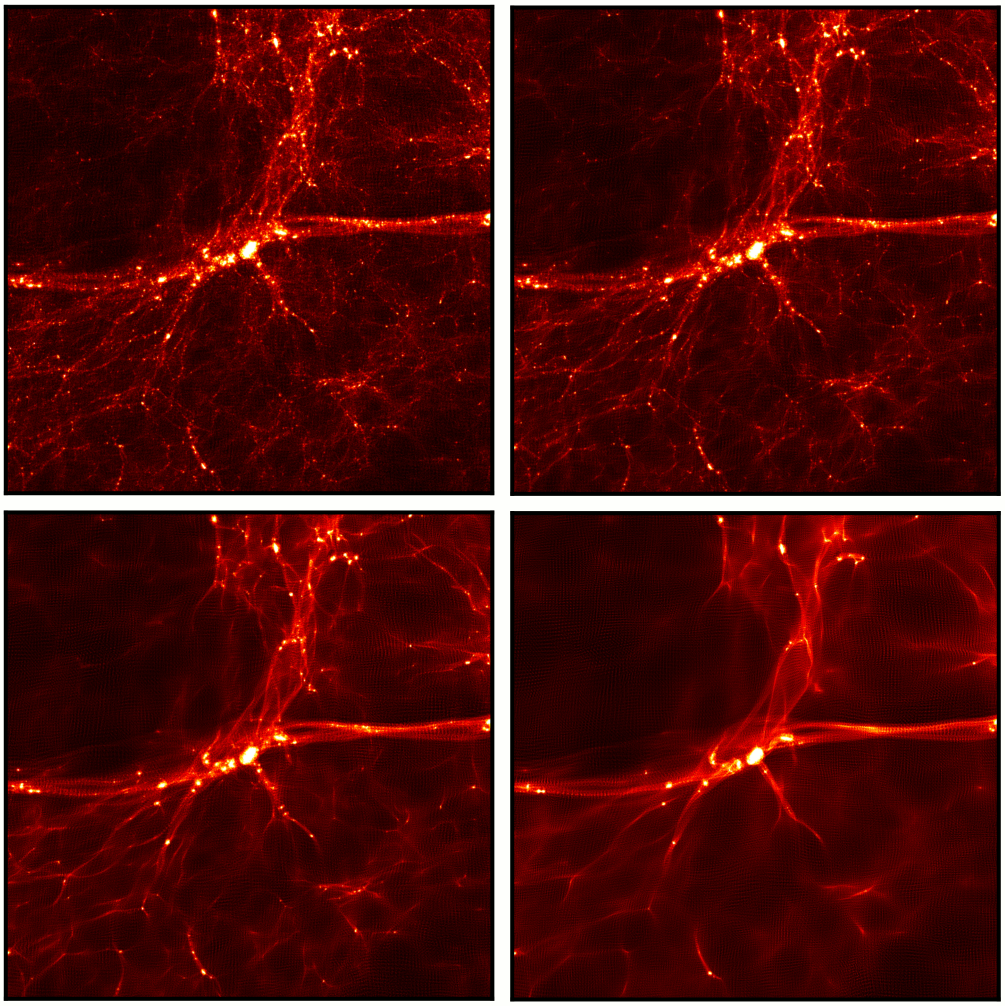

Figure 2. Simulation images for CDM and WDM at z=6, each initialized with the same random seed. The panels are $10h^{-1}$Mpc square and 6 h^{-1}Mpc deep; they are centered on the most massive halo in the box. The upper left panel is CDM, with 2.6 keV WDM in the upper right. The bottom panels correspond to WDM: 1.3 keV (left) and 0.8 keV (right). The lack of structure for the lightest WDM models is striking compared to CDM.

$1/\bar{n}V$ where V is the simulation volume and $\bar{n}$ the number count. However, for smaller halo masses, shot noise is dwarfed by sample variance (Hu & Kravtsov 2003). The average density in the simulation volume may happen to be an over- or under-dense part of the universe, and since haloes are biased tracers of the density field, this will lead to differences in the halo mass function. The best way to correct this is to run independent samples of the underlying density field (different seeds for the initial conditions), but this comes at a considerable cost in terms of CPU hours. Alternatively, the sampling variance can be estimated by analytic methods as given by equation (4) in Hu & Kravtsov (2003), with a Sheth-Tormen bias for example. However, such a bias is based on fits to ΛCDM simulations. It seems plausible that such a bias would not change significantly if used in a WDM cosmology as it is primarily determined by nature of halo collapse, but to avoid any complications with the error estimate, we directly calculate the sample variance in the halo mass function by the jackknife technique. We do not consider any contributions to the halo mass function from scales larger than the simulation box, since we are mostly interested in the low mass end, and the simulated volume is significantly larger than the scale of clusters at the redshifts of interest.

Finally, below a specific mass scale dependent on numerical resolution, it has been well established that WDM produces artificial haloes in simulations (Wang & White 2007; Angulo et al. 2013), an effect of the shot noise due to the finite particle count. These haloes are usually visible as regularly spaced clumps in the filaments of the cosmic web, and they form below a mass scale proportional to $m_p^{-1/3}$, where m_p is the simulation particle mass. However, force resolution also plays a role, and an excessive force resolution, as compared to the mass resolution, can increase the number of artificial haloes (Angulo et al. 2013). Schneider et al. (2013) showed that the artificial haloes can be modeled by a power law increase in the WDM halo mass function below the mass scale. Most attention has been given to correcting the halo mass function for low redshift, since contamination of the halo population is the largest here, due to the fact that the artificial haloes have had more time to form and accrete.

There have been no focused studies on artificial halo contamination is at redshifts $z \gtrsim 5$. In the results presented below, down to the halo mass scale adopted for our completeness limit, we see little if any indication of a low-mass upturn in our WDM halo mass functions; such an upturn would be indicative of significant artificial halo contamination. Moreover, since any artificial haloes present would provide an increase in the halo mass function (thus making

WDM more like CDM) ignoring them only makes our WDM constraints more conservative. In what follows, we have conservatively chosen to ignore any corrections for artificial haloes in our catalogs.

Figure 2 provides a qualitative depiction of the differences inherent in WDM compared to CDM simulations. Shown are $10 \times 10 \times 6$ (comoving h^{-1}Mpc) slices of each of our simulation volumes, centered on the most massive halo at a redshift of $z = 6$. On large scales the slices look similar, but on smaller scales there is a clear lack of structure in the WDM models.

2.3 Halo catalogs

We used the Amiga Halo Finder (AHF, Knollmann & Knebe 2009) to identify haloes in our simulations. The halo mass M_h used in this work is calculated using the over-density ($\Delta_{\rm vir}$) formula from Bryan & Norman (1998) for our cosmology at each specific redshift. Note that our conclusions do not change when using different over-density definitions, e.g. $\Delta_{200} = 200\rho_{\rm crit}$. As explained above, to build our mass luminosity relation using the abundance matching technique we took into account the merger history of each halo and used its maximal mass obtained over its lifetime $M_{\rm peak}$ instead of M_h. In any case, this correction turned to be small due to the lack of substructure at high redshifts. We used a requirement of at least 40 simulation particles to constitute a halo, setting a halo mass completeness limit of $M_h = 3.4 \times 10^8\, h^{-1} M_\odot$.

Compared to the density maps shown in Figure 2, the differences between WDM and CDM become even more apparent when we compare halo counts. Figure 3 shows two of the same density slices overlaid with white circles to indicate identified dark matter halos more massive than our $M_h = 3.4 \times 10^8\, h^{-1} M_\odot$ completeness limit. Circle sizes are proportional to the virial radius of each identified halo. The difference in collapsed structures is striking between these two simulations. For example, the void in the upper left corner is completely empty of any haloes in the 0.8 keV WDM run.

Figure 4 provides a more quantitative demonstration of the differences in halo abundances from model to model, where each panel shows the cumulative dark halo mass function at redshifts $z = 6$, 7, 8, and 13. The CDM result (dotted line with shading) is in all cases above the WDM models (solid lines with shading, as labeled). Angulo et al. (2013) found a suppression of the halo mass function of the form[1]

$$\frac{n_{\rm WDM}}{n_{\rm CDM}}(M) = \frac{1}{2}\left(1 + \frac{M_1}{M}\right)^{-\alpha}\left[1 + {\rm erf}\left(\log\frac{M}{M_2}\right)\right]. \quad (5)$$

We have verified this expression provides a good fit to the WDM/CDM abundance ratio for $z \lesssim 10$, with decreasing accuracy with increasing redshift. In our simulations, at $10^9 M_\odot$, the 0.8 keV model is suppressed by more than an order of magnitude at all redshifts relative to CDM.

As can be seen in the $z = 13$ panel of Figure 4, no haloes at all exist in 0.8 keV WDM model. Indeed we find that no haloes have formed before $z = 12$ for 0.8 keV WDM and none before $z = 15$ in the 1.3 keV model. Detections at these epochs should be robust in the future with JWST. However, even current detections offer an interesting test: the point with error bar (2σ) corresponds to the *lower limit* on the cumulative abundance of galaxies at those redshifts, as set by the faintest galaxies observed in the HUDF (Bouwens et al. 2007; McLure et al. 2012; Oesch et al. 2013). Its horizontal position (corresponding halo mass) is based on the luminosity limit and our adopted M_h-L relation presented in the next section. Importantly, the total abundance of galaxies at each redshift must be above the data point shown (regardless of its horizontal positioning on the plot). One can see without any further analysis that the 0.8 keV WDM model will have trouble producing enough galaxies to match *current* observations at $z > 8$; there are simply not enough collapsed objects of any mass to account for the known galaxies at this epoch. The viability of the other WDM models is not immediately apparent from figure 4 in itself, since the halo mass function is not directly observed.

In order to provide a more precise connection with observations we will need a mapping between halo mass and galaxy luminosity. This is a primary subject of the next section.

[1] Strictly speaking Angulo et al. (2013) has $\alpha = 1$ fixed, however they also correct for artificial haloes. We find that keeping α as a free fitting parameter is necessary to provide reasonable fits, probably owing to a strong evolution with redshift.

3 PREDICTING OBSERVABLES

3.1 Observed Luminosity Functions

We will normalize our predictions using observed high-z galaxy counts. In doing so, we follow the literature and assume that high-z luminosity function is well characterized by a Schechter function

$$\phi(L)\, dL = \phi_* \left(\frac{L}{L_*}\right)^{\alpha} \exp\left(-\frac{L}{L_*}\right) \frac{dL}{L_*}. \quad (6)$$

Robust observations of luminosity functions with measures of ϕ_*, L_*, and α exist out to $z \sim 8$ (Bouwens et al. 2011; McLure et al. 2012; Schenker et al. 2013) and current observations can provide constraints on the normalization (with other parameters fixed) out to $z \sim 10$ (Oesch et al. 2013).

We parameterize the evolution of the luminosity function with redshift by fitting quoted observational results for $\log\phi_*$, L_* and α and fitting them linearly as a function of z from $z = 4 - 8$. Figure 5 shows the fit used in this work in comparison with fits from other authors. The data points used for this fit (plotted) are taken from Bouwens et al. (2007) for $z = 4 - 6$ and from McLure et al. (2012) for $z = 7 - 8$. Points at higher z (which assumed fixed values for α and ϕ_*) are shown for reference from Oesch et al. (2013). Note that formally the luminosity density becomes divergent if $\alpha < -2$, however, due to the introduction of a minimum cutoff scale in halo masses in equation (12) this is not a cause for concern. It is important to stress here that even small changes in the fit parameters provides drastic changes in the reionization history. This is especially true for changes to the faint end slope α of the luminosity function (Bouwens et al. 2011). Future observations from the JWST can hopefully much better constrain α at high redshift.

3.2 Connecting Halos to Galaxies

In assigning luminosities to dark matter halos we assume that brighter galaxies reside in more massive halos and that the relationship between halo mass and galaxy luminosity is monotonic, following the same relation for all dark matter models.

Fundamentally we rely on the abundance-matching technique (Kravtsov et al. 2004; Vale & Ostriker 2004), which defines the relationship between halo mass and galaxy luminosity (or alternatively stellar mass) by equating the cumulative number density of halos to the cumulative number density of galaxies observed. The power of this approach is that the observed luminosity function is

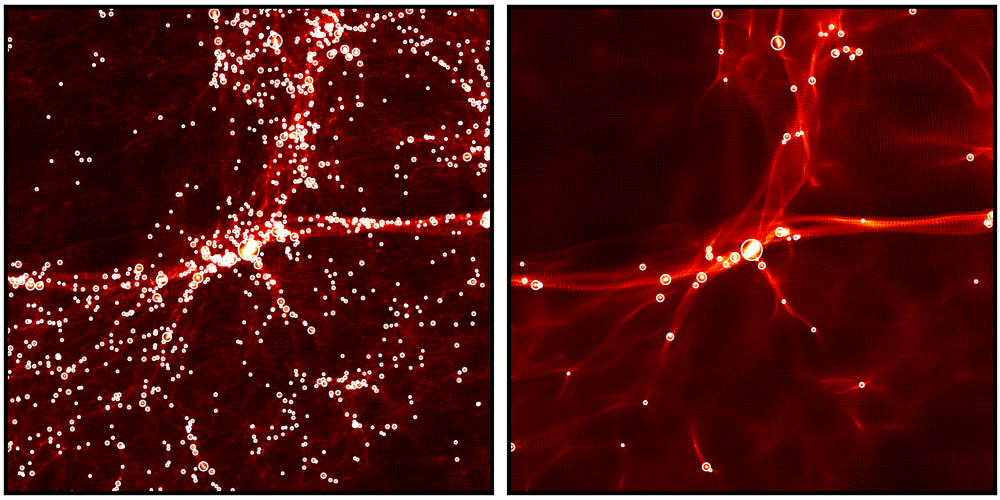

Figure 3. Simulation snapshots from CDM (left) and 0.8 keV WDM (right) overlaid with circles to indicate identified dark matter halos that are more massive than $3.4 \times 10^8 h^{-1} M_\odot$. The size of the circle is proportional to the virial radius of each halo. The CDM slice is filled with collapsed structure at z=6, while the WDM slice is largely devoid of collapsed halos that are massive enough for hydrogen cooling. Note that artificial haloes would show up as regularly separated haloes in the filaments, suggesting that contamination by artificial haloes is likely negligible here.

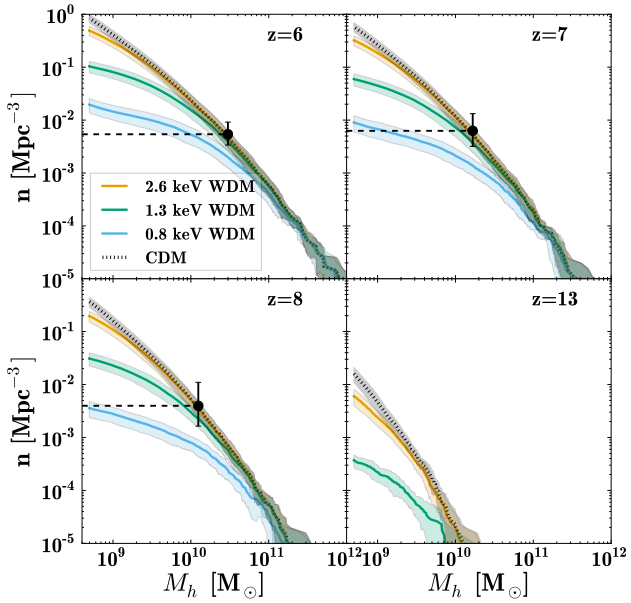

Figure 4. Shown are cumulative halo mass functions at selected redshifts for our CDM and WDM simulations. Notice how the suppression of WDM increases with z. At $z > 12$ no dark matter haloes are identified at all in the 0.8 keV WDM model. The central lines denote the simulated halo mass function, while the shaded areas indicate jack-knife uncertainties. The horizontal dashed lines correspond to the known *lower limit* on the cumulative galaxy abundance at each redshift based on the faintest HUDF observations; assuming that galaxies reside in halos, any viable mode must produce a total abundance of halos above this line. The point with 2σ error bar is placed at the halo mass corresponding to the HUDF luminosity limit as inferred from abundance matching, discussed in Section 3. For constraints, we use the values of the galaxy luminosity functions observed and inferred from the halo abundance matching method, shown in figure 7.

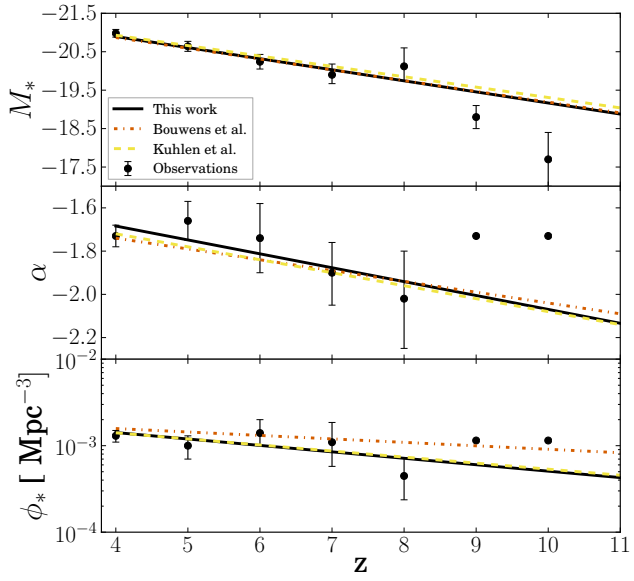

Figure 5. Shown are the fits for the Schechter function parameters M_*, α and ϕ_*. The black symbols show observed values with quoted uncertainties (Bouwens et al. 2007; McLure et al. 2012; Oesch et al. 2013). The lack of uncertainties for ϕ_* and α at $z = 9$ and 10 is due to the fact that they were fixed in the estimation of M_*. Since there is a large correlation between α and M_*, these observations were not used for the fit. See Oesch et al. (2013) for further discussion. The solid black line is the fit used in this work, and we show other fits from Bouwens et al. (2011) and Kuhlen & Faucher-Giguere (2012) for comparison. Note that our fit uses newer observations from the 2012 HUDF results than the comparison fits. For reference, our fits are $\log \phi(z) = -2.6 - 0.074z$, $M_*(z) = -22.1 + 0.29z$, and $\alpha(z) = -1.4 - 0.064z$.

fully reproduced (at least down to luminosities where the observations are complete or to where the matching is performed) while sweeping all uncertainties galaxy formation physics under the rug. In principle other halo parameters could be used as the rank order of

choice (e.g., maximal circular velocity Trujillo-Gomez et al. 2011). Recently, Behroozi and collaborators have argued that halo mass is the most robust variable to use for these purposes (Behroozi et al. 2013).

Specifically, we set the relationship between halo mass M_h and UV luminosity L at different redshifts z via

$$n_{\rm CDM}(M_h, z) = \Phi_{\rm gal}(L, z)\,, \tag{7}$$

where $n_{\rm CDM}$ is the cumulative dark halo count in CDM and $\Phi_{\rm gal}$ is the cumulative luminosity function as given by the Schechter function fits discussed in section 3.1. The resultant relationships at various redshifts are plotted in Figure 6. As can be seen, we are fundamentally assuming that the relationship between halo mass and galaxy luminosity obeys a power-law at faint magnitudes (normalized at the bright end by observations) with $M_h \propto L_{AB}^a$, $a \approx 0.75$ (or $\log M_h \sim -0.3 M_{AB}$).

Our fundamental assumption is that the halo mass-luminosity mapping is a power law at faint magnitudes. Furthermore we are conservatively assuming that the relationship between halo mass and galaxy luminosity is the same in CDM and WDM (obeying near power-law behavior at faint luminosities). This approach demands that all models match the observations at the bright end (where halo counts overlap), and makes the assumption that there is no special break (towards more efficient galaxy formation) in the luminosity-halo mass relation in WDM for small halos. This is conservative because there is no reason to expect that WDM halos will be more efficient at making galaxies than CDM halos. Indeed, WDM halos collapse later and have had less time to form stars, so we might expect them to be less efficient at forming stars than their CDM counterparts.

Herpich et al. (2013) performed hydrodynamical simulations of several different WDM cosmologies. They found only slight differences between the stellar masses of the different dark matter models they considered, and the difference they did see was towards less efficient formation in WDM as discussed above. For the most extreme case, comparing a 1 keV WDM model to CDM, they found a ratio of $M_{\star,\rm CDM}/M_{\star,\rm WDM} \sim 2$ in stellar masses at $z = 0$. Therefore, the main differences in the star formation histories are produced at late times, and therefore this relatively small effect is more reduced at the high redshifts of interest for this work. Small variations in the stellar feedback implementation have a much greater impact on the final stellar mass of a galaxy than WDM particle mass. While the results of Herpich et al. (2013) are based on low-z simulations it seems reasonable to expect the same to be true at higher redshift. Appendix A further elaborates on using the CDM halo catalogue as the fiducial model.

The assumption that the power law behaviour for the faint end of the halo mass-luminosity mapping translates into a suppression of the luminosity function in the corresponding WDM model. This suppression is then exactly equal to the ratio of the halo catalogues at the given mass scale, which is an aggressively conservative assumption of a cancelation of two disparate physical mechanisms. Furthermore, this requires that the WDM luminosity functions diverge from a pure Schechter fit. We stress that several other processes could also cause the luminosity function to diverge from a power law, however, since no such divergence is yet observed, this translates into constraints on the nature of dark matter.

Before moving on we note that while the general abundance-matching approach has proven successful and robust at reproducing galaxy properties in the low redshift universe, it is less well tested at higher redshifts. For example, the scatter at fixed halo mass appears to be fairly minimal at low-z (Behroozi et al. 2013) and the relationship between halo mass and luminosity is well described by a power law for faint systems (Moster et al. 2013; Garrison-Kimmel et al. 2013). At high redshift however, the relationship between halo mass and UV luminosity could in principle exhibit significant scatter, though a power-law relationship for the smallest galaxies appears consistent with the data (Behroozi et al. 2013). We adopt a strict one-to-one relationship between halo mass and UV luminosity as a starting point in investigating the expected differences between CDM and WDM on galaxy counts in the high-z universe. Because we are looking at differential effects between the two models, driven by the declining number of low-mass halos in WDM, we anticipate that this approach provides a fair starting point, though it would be useful to extend this approach to more complicated mappings in the future.[2]

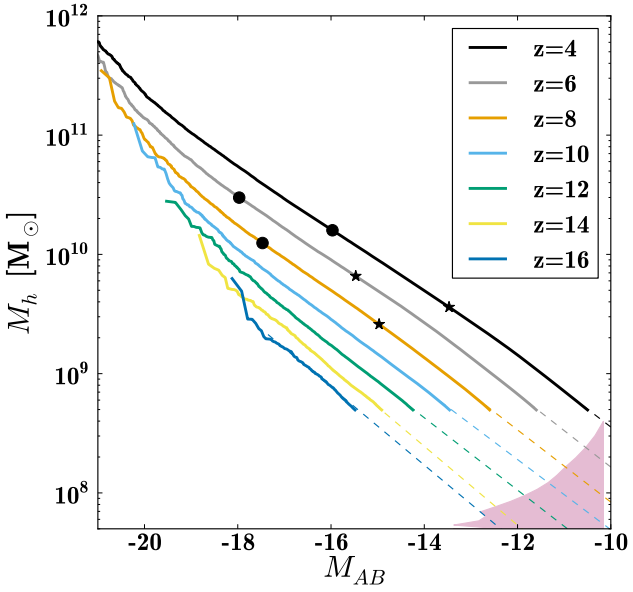

Figure 6. Shown is the relationship between halo mass and galaxy magnitude adopted in this work. The solid lines are derived from our simulations using abundance matching as described in the text. They are truncated at the point where are dark matter halo catalogs become incomplete. The dashed lines are power law extrapolations, fit to the solid lines at the faint end as $\log M_h = C + b\, M_{AB}$, with resulting slopes of $b = -0.35$ to -0.30. The shaded area is an estimate of the cooling limit for halos, below which galaxies cannot form efficiently, via equation (12). The circles indicate the current HUDF magnitude limit, the asterisks are the expected JWST limits.

3.3 Reionization

With predictions for luminosity functions in hand, we can directly connect those to expectations on reionization. Star forming galaxies at $z \gtrsim 6$ are the primary candidate for the main process driving the reionization of the intergalactic medium (IGM). Changes in the abundance of early galaxies therefore translates into different reionization histories.

The reionization process is a tug-of-war between ionizing radiation from short-lived massive stars and atomic recombination

[2] Notably, we take the inherent scatter in the halo mass-luminosity mapping into consideration.

in the IGM. In terms of the volume filling fraction of ionized hydrogen $Q_{\rm HII}$ this is captured in the differential equation (Kuhlen & Faucher-Giguere 2012)

$$\frac{dQ_{\rm HII}}{dt} = \frac{\dot{n}_{\rm ion}}{\langle n_H \rangle} - \frac{Q_{\rm HII}}{\bar{t}_{\rm rec}} \,, \tag{8}$$

where $\dot{n}_{\rm ion}$ is the creation rate of ionizing photons, and $\langle n_H \rangle$ is the comoving density of baryons

$$\langle n_H \rangle = X_p \Omega_b \rho_{\rm crit} \,, \tag{9}$$

and $\bar{t}_{\rm rec}$ the mean time of HII recombination

$$\bar{t}_{\rm rec} = \frac{1}{C_{\rm HII} \alpha_B(T_0) \langle n_H \rangle (1 + Y/4X)(1+z^3)} \,. \tag{10}$$

Here α_B is the case B recombination coefficient[3], T_0 is the IGM temperature and X and $Y = 1 - X$ are the primordial hydrogen and helium abundances respectively. Since recombination is not isothermal and uniformly distributed, the gas clumping factor $C_{\rm HII} = \langle n_H^2 \rangle / \langle n_H \rangle^2$ is also introduced to quantify the effects these approximations have. Allowing a fraction of $f_{\rm esc}$ of the produced ionizing photons to escape the gas clouds where the massive stars are born, the injection of UV photons into the IGM is given by the differential luminosity function ϕ down to a limiting luminosity $L_{\rm lim}$

$$\dot{n}_{\rm ion} = \zeta_{\rm ion} f_{\rm esc} \int_{L_{\rm lim}}^{\infty} L \phi(L) dL = f_{\rm esc} \zeta_{\rm ion} \rho_{UV} \Big|_{L_{\rm lim}} \,. \tag{11}$$

Here $\zeta_{\rm ion}$ is a parameter converting the galactic UV luminosity to ionizing photon luminosity, or more precisely the amount of Lyman continuum photon emission per 1500 Å unit UV luminosity density. Note that $f_{\rm esc}$ and $\zeta_{\rm ion}$ are completely degenerate parameters, as reionization is only sensitive to the product. Any change in one of these parameters could be attributed to the same relative change in the other.

Critical in this analysis is what value to assign to the limiting luminosity in equation (11), that is, the minimal UV luminosity expected possible from early galaxies. Naively, one might expect no such lower limit. However, to capture the hot primordial gas needed for star formation, a sufficiently deep potential well is required. This effectively puts a lower bound on the possible UV luminosities (and therefore halo masses) due to photo-evaporation. Furthermore, star formation can only take place once the hot gas has cooled sufficiently, and this introduces a limiting mass threshold below which stars cannot form. In this work we only consider the cooling limit for halo masses, and we use the parameterization adopted by Sobacchi & Mesinger (2013)

$$M_{\rm cool} = 10^8 \left(\frac{1+z}{10} \right)^{-3/2} M_\odot. \tag{12}$$

The shaded red area in Fig. 6 shows an estimate of the region where galaxy formation is suppressed owing to this cooling limit, effectively mapping the halo mass limit to a luminosity cutoff. Based on this, we will explore cutoff magnitudes between $M_{AB} = -10$ and $M_{AB} = -13$ in what follows.

[3] Commonly used case A and B definitions differentiate mediums that allow the Lyman photons to escape or that are opaque to these lines (except Lyman-α) respectively. Case B is most appropriate for this reionization calculation.

An important constraint on reionization comes from the Thomson optical depth to the CMB,

$$\tau_e = \int_0^{z_R} \frac{c(1+z)^2}{H(z)} Q_{\rm HII} \sigma_T \langle n_H \rangle \left(1 + \eta(z) Y/4X\right). \tag{13}$$

Here z_R is the redshift of recombination, σ_T is the Thomson cross section and $\eta = 1$ when Helium is singly ionized and $\eta = 2$ when Helium is doubly ionized after $z \lesssim 4$.

In this work, we do not include an evolution in the reionization parameters. Kuhlen & Faucher-Giguere (2012) found that for their best fit scenario, evolution in the limiting luminosity alone is not enough to match both Lyα constraints and reionization constraints, and the data provides no conclusive evidence for an evolution in any case. Evolution in $f_{\rm esc}\zeta_{\rm ion}$ (resulting perhaps from evolution in the stellar initial mass function) may be more plausible. We will present our results with different values of $f_{\rm esc}\zeta_{\rm ion}$ and limiting luminosity, but they will remain fixed with redshift. Evolution in the clumping factor $C_{\rm HII}$ may be expected, but no definitive determination of its evolution exists. For example, Finlator et al. (2012) presents a detailed analysis of the evolution, suggesting that the clumping factor rises from $C_{\rm HII} < 1$ for $z > 10$ to $C_{\rm HII} \sim 3.3$ at $z \sim 6$. It should be noted that our model equation (8) does not include the detailed distribution of hydrogen where some dense clumps reionize later than less dense clumps. This simplification is likely inaccurate in the final phase of reionization around $z \sim 6$, however we expect it to be an appropriate approximation on average for higher-z and in the large cosmological volumes of interest here.

In what follows we adopt the reionization parameters $C_{\rm HII} = 3$, $\zeta_{\rm ion} = 10^{25.3}{\rm ergs}^{-1}{\rm Hz}$, $X_p = 0.75$, $T_0 = 2 \times 10^4{\rm K}$ and $\alpha_B = 1.6 \times 10^{-13}{\rm cm}^3/{\rm s}$. The escape fraction and limiting luminosities vary, and will be indicated in the relevant figures.

4 RESULTS

Here, we explore the constraints on WDM models by direct number counting and the inferred reionization history, and illustrate how future galaxy count surveys can improve these constraints on WDM models.

4.1 WDM Constraints from Galaxy Counts

As explained in section 3.2, given our (conservative) assumption of the star formation efficiency being the same in the different dark matter models, deviations in the implied WDM luminosity function from the observed Schechter fit translates into constraints on the WDM model.

Figure 7 shows the implied luminosity functions for CDM (dotted black) and each of our WDM models (solid, colors indicated). The symbol with error bar is the known (observed) cumulative count of galaxies at the faint HUDF limit, with errors indicative of the 2σ uncertainty calculated as in Fig. 4. The shaded band corresponds to a 1σ uncertainty of the observed best fit Schechter function (seen in figure 5), extrapolated down to an approximate JWST deep field limit (indicated by the vertical line). We see clearly here that the 0.8 keV WDM model (solid cyan) is strongly disfavored by current observations of the galaxy luminosity functions. The 1.3 keV model, while currently consistent with observations, demonstrates significant deviations from CDM at $z = 13$ at magnitudes observable with JWST. Deep galaxy counts at this and earlier epochs may be even sensitive to 2.6 keV WDM.

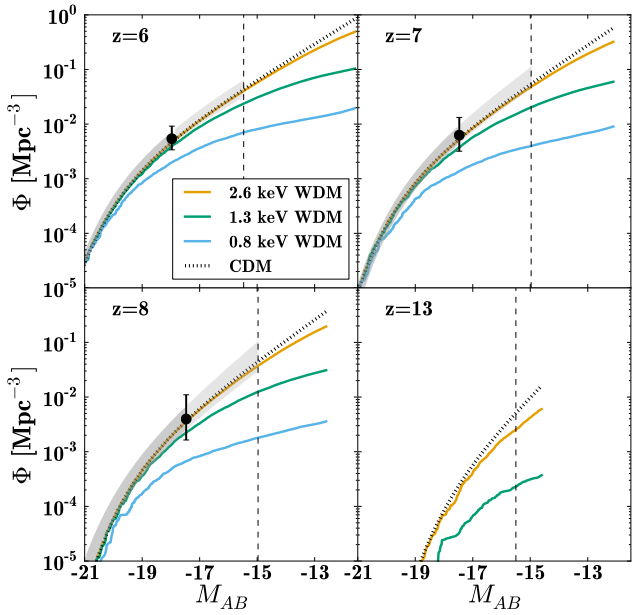

Figure 7. Shown are cumulative luminosity functions for our CDM and WDM models at various redshifts (comoving volumes). In each panel, the symbol with error bar marks the observed cumulative count at the limit of published HUDF luminosity functions with 2σ uncertainties shown. The shaded bands bands correspond to 1σ uncertainties, and the vertical line marks the approximate reach of a hypothetical deep field observation with JWST. For redshifts where the luminosity function has been observed by HUDF the JWST limit has been assumed to be 2.5 magnitudes fainter. For $z = 13$ a limit of -15.5 has been assumed (see Windhorst et al. (2006)). The 0.8 keV WDM model is heavily disfavored by current observations, and the 1.3 keV model is marginal. At redshift $z = 13$, JWST observations will likely be able to rule out 1.3 keV WDM and perhaps be sensitive to 2.6 keV.

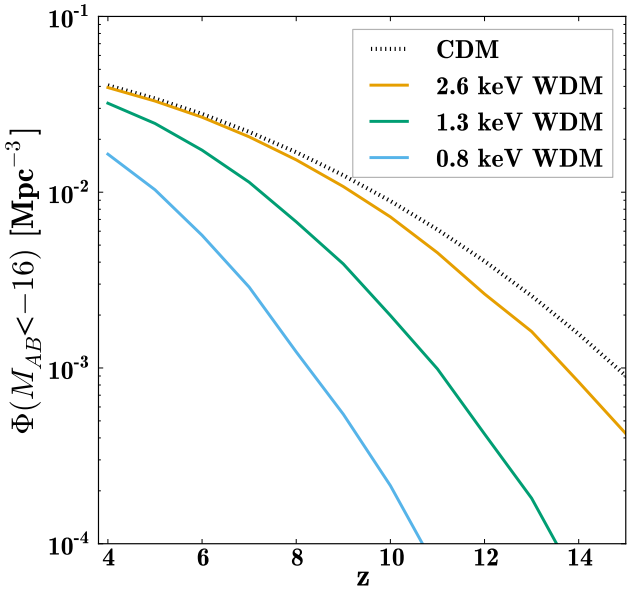

Figure 8. Predicted number density of galaxies brighter than $M_{AB} = -16$ as a function of redshift for our CDM and WDM models. JWST should be capable of detecting galaxies of this brightness across the redshift range plotted, and perhaps be sensitive to differences between 2.6 keV WDM and CDM at $z > 12$.

We quantify how much the different models are disfavored with a χ^2 test,

$$\chi^2 = \sum_i \left(\frac{\Phi - \Phi_{\rm obs}}{\sigma} \right)^2 . \quad (14)$$

Here $\Phi_{\rm obs}$ is the abundance at the faint-end limit from observed luminosity functions (Bouwens et al. 2007; McLure et al. 2012; Oesch et al. 2013) and σ is the error on the simulated luminosity function, which is given by the jackknife error on the halo mass function at the corresponding abundance.[4] The CDM luminosity function is a fit to the redshift evolution of the Schechter function parameters (shown in Fig. 5) based on current observations, and not the actual quoted fits at each redshift, and this produces a small but non-zero $\chi^2 = 2$ for the CDM case with 5 degrees of freedom (corresponding to the observations from $z = 4$ to $z = 8$) from the luminosity functions (85% consistency). The χ^2 for the 2.6, 1.3 and 0.8 keV models are 2.27, 14.4 and 372, respectively, with probabilities for these models at getting the observed luminosity functions of 81%, 1.3% and $\ll 10^{-10}$. Therefore, the 1.3 keV WDM model is disfavored at approximately 98.6% C.L. (2.2σ), and the 0.8 keV WDM model is disfavored at very high significance, $> 10\sigma$. Note that the statistical methods in the modeling and constraints here do not reflect systematic uncertainties in the halo abundance matching method. Because we arrive at a consistent and smooth power law relation for the abundance matching, the systematic effects are likely small, though difficult to quantify.

Had we considered WDM artificial halos and the fact that the star formation efficiency is slightly lower in WDM than in CDM the constraints would improve slightly, since there would then be fewer and less luminous galaxies. However, these effects are not likely to be very important at redshifts $z \geqslant 4$, and are *a priori* unknown.

Faint galaxy counts at even higher redshift will be particularly sensitive to WDM models. We demonstrate this in Figure 8. Here we show the cumulative number density of galaxies brighter than $M_{AB} = -16$ as a function of redshift for each of our models. The differences between CDM and WDM are significant, especially for the lower mass WDM cases. Deep JWST observations should be sensitive to galaxy detections at least this faint out to $z = 15$, and therefore will provide a direct probe of the small-scale power spectrum by counting galaxies.

4.2 WDM Constraints from Reionization

Fundamental to the ability of galaxies to reionize the universe is the production rate of ionizing photons, $\dot{n}_{\rm ion}$, which is proportional to the total UV luminosity density, ρ_{UV}, coming from these sources (see equation 11). For an underlying galaxy luminosity function with a steep faint-end slope α, the total luminosity density implied will be sensitive to the assumed faint-end cutoff used to calculate ρ_{UV}. Figure 9 shows the luminosity density in our models as a function of faint-end cutoff at selected redshifts. Because WDM models have flatter faint-end luminosity function slopes, the total

[4] We use the jackknife errors instead of the errors on the observed luminosity function, since they are larger (shown in Fig. 7). The χ^2 test here is approximate, but our conclusions are robust regarding the models' consistency.

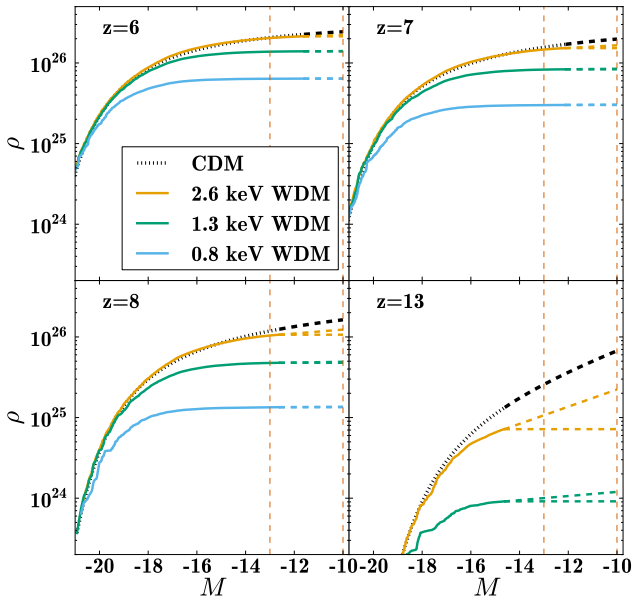

Figure 9. The cumulative UV luminosity density (in units erg/s Hz^{-1} Mpc^{-3}) as a function of magnitude cutoff at selected redshifts for the dark matter models considered. The vertical lines mark the two cutoff scales we consider in this paper as plausible for extending the galaxy luminosity function. The change from solid to dashed lines occurs at the magnitude corresponding to the resolution limit of the simulation, beyond which we rely on extrapolations (dashed) to predict faint galaxy contributions. For a given WDM model, the upper dashed lines extend the best-fit power-law of the resolved function. The lower dashed line marks the constant value at the faintest simulated point, as would be expected if the WDM halo mass function drops dramatically beyond this point. These two extremes bracket reasonable expectations.

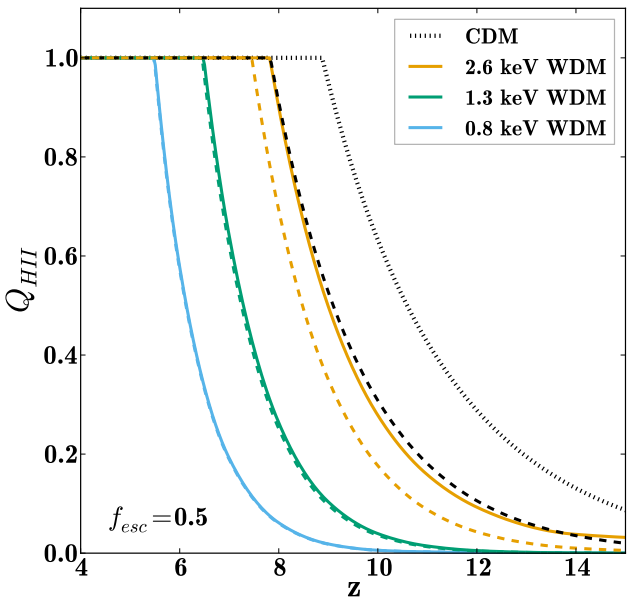

Figure 10. Buildup in volume filling fraction of ionized hydrogen as a function of redshift for our CDM and WDM models assuming $f_{\rm esc} = 0.5$ and with limiting integration magnitudes of $M_{AB} = -10$ (fiducial lines, as in caption) and $M_{AB} = -13$ (dashed). The WDM models produce more rapid buildups at later times compared to CDM. The 0.8 keV WDM model does not complete reionization by $z \sim 6$ (as seems to be required by observations) regardless of the assumed faint-end cutoff.

ρ_{UV} is less sensitive to the faint-end cutoff, i.e. the implied cumulative ρ_{UV} values flatten relative to CDM at fainter magnitudes. Importantly for our considerations, WDM predictions for reionization will be less sensitive to the adopted faint-end cutoff than CDM, owing to the lack of small galaxies in these models.

The points where the lines change to dashed in Fig. 9 mark the resolution limit in the simulations. The two WDM dashed lines bracket the following extreme cases: one, a power law fit to the faint end, and, two, the constant value at the faintest point resolved in the simulations. The actual luminosity density would be somewhere between these two extremes, though for the 0.8 keV and 1.3 keV models the difference is negligible. All our analysis utilizes the power law extrapolations to get conservative estimates.

With the luminosity density in hand, the reionization history can now be determined by virtue of equation (8). Fig. 10 presents the volume filling fraction $Q_{\rm HII}$ as a function of redshift for two choices of limiting magnitude in calculating the luminosity density. The fiducial line types (shown in the legend) correspond to a limiting magnitude of $M_{AB} = -10$ while dashed lines cut off at a brighter limit of $M_{AB} = -13$. We used the initial condition $Q_{\rm HII} = 0$ at $z = 20$ and integrated forward in time. We choose an optimistic escape fraction of $f_{\rm esc} = 0.5$, higher than assumed in both Robertson et al. (2013) and Kuhlen & Faucher-Giguere (2012), and therefore more conservative with respect to WDM model constraints since we use the same $\zeta_{\rm ion}$ as in Kuhlen & Faucher-Giguere (2012). Robertson et al. (2013) uses a lower $\zeta_{\rm ion}$, but instead assumes an almost constant luminosity density at the cutoff scale at high redshift.

All of the models in Figure 10 except 0.8 keV WDM have completed reionization by $z \sim 5.8$ as required by results inferred from the kinematic Sunyaev-Zeldovich effect and CMB polarization observations (Zahn et al. 2012). For the 0.8 keV model shown, reionization is complete at $z = 5.5$. In general, the WDM cases produce a more rapid late-time buildup of ionized hydrogen due to the high redshift suppression of haloes. It can also be seen that the difference between CDM and 2.6 keV WDM is larger when the fainter limiting magnitude is used, simply because the difference between the models is much larger here. Of course, these results are sensitive to the escape fraction. For example, if an escape fraction of $f_{\rm esc} = 0.2$ is used for the 1.3 keV model full reionization is not reached until $z = 5.4$ (not shown on figure), so fairly high escape fractions seem to be required for 1.3 keV to reach full reionization by $z \sim 6$.

Another important probe of reionization is the integrated optical depth of electron scattering from the CMB. The shaded bands in Figure 11 show the CMB optical depth range of 0.092 ± 0.013 from the most recent *Planck* results (Ade et al. 2013). The lines show predictions for the optical depth as contributed as a function of redshift for our WDM and CDM models assuming an escape fraction $f_{\rm esc} = 0.5$, with the two panels corresponding to different limiting magnitudes. Interestingly, with this choice of (fairly high) escape fraction, none of our WDM models can reproduce the measured optical depth, and even CDM requires a luminosity function extrapolation to a very faint limiting magnitude. This is consistent with the findings of Robertson et al. (2013).

In Fig. 12, we show results for the optical depth, now assuming $f_{\rm esc} = 1$. In this case, the 2.6 keV model can reproduce the

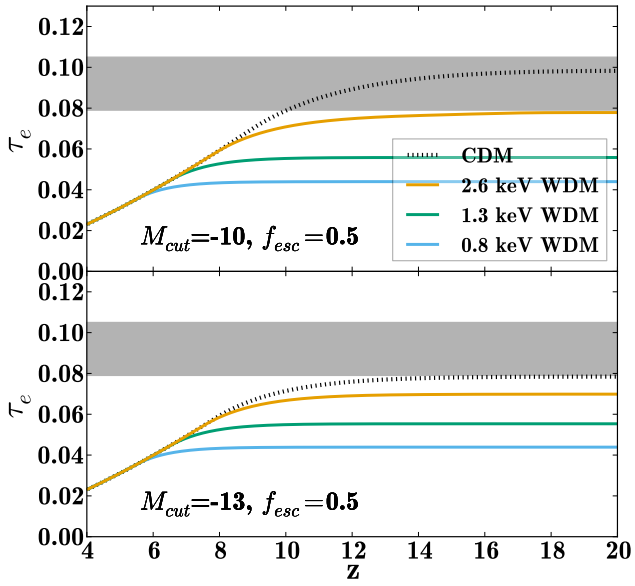

Figure 11. The electron-scattering optical depth of the CMB predicted for our CDM and WDM models, with the contribution shown cumulatively as a function of redshift. The top panel shows results for an assumed luminosity function cutoff at $M_{AB} = -13$ and the bottom panel extends this cut to very faint luminosities $M_{AB} = -10$. In all case we assume $f_{\rm esc} = 0.5$ and our fiducial value of $\zeta_{\rm ion}$. The bands are the 68% confidence limit on the most recent *Planck* results Ade et al. (2013). Note that none of the WDM models reach within the 68% confidence band from *Planck*.

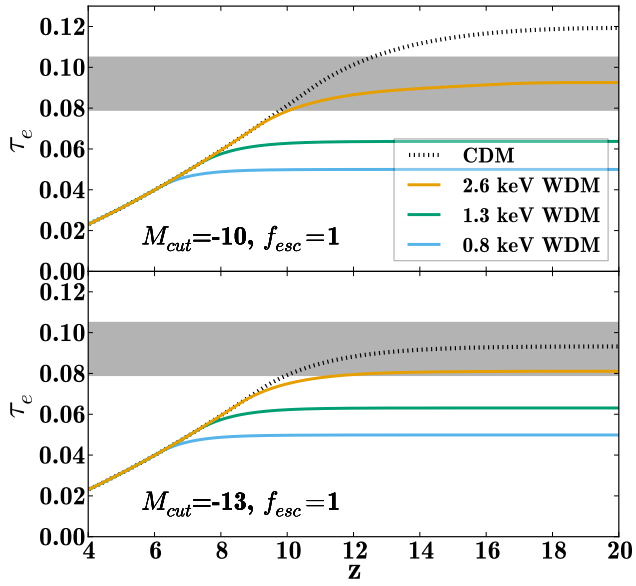

Figure 12. Electron-scattering optical depth as in Fig. 11 except now assuming $f_{\rm esc} = 1.0$. Even with fairly extreme assumptions, neither of the two lightest WDM models are able to reach the 68% confidence range (bands) reported by *Planck*.

Planck value, though a fairly faint limiting magnitude seems to be required, even in this extreme case. Unsurprisingly, CDM severely overshoots the optical depth with these (rather high) reionization parameters. It is noteworthy that neither of the low mass WDM models can reproduce the Planck optical depth within its 68% confidence interval, even with very optimistic choices. If these WDM models are to be viable in the face of reionization constraints, they would require either significant contribution to the ionizing flux from non-stellar sources, or a significantly larger combination of $f_{\rm esc}\zeta_{\rm ion}$ than what is currently believed to be realistic. A smaller $C_{\rm HII}$ could also help in this respect. Future observations will likely better constrain these parameters.

5 DISCUSSION

Future measurements of the luminosity function of faint galaxies at high-z, particularly those from JWST, and possibly with HST via the Frontier Fields initiative, will significantly improve the sensitivity to WDM models and the halo mass cutoff effects presented here. For a direct number count comparison the mass resolution of our simulations is sufficient to connect with observations down to plausible detection limits with JWST.

In contrast, our results on reionization specifically for the 2.6 keV model would improve with greater mass resolution. This is because of our conservatively approximated increasing faint end luminosity density function, which likely flattens at low luminosities in this model, but remains unresolved in our simulations. This improvement can also be made, though to a lesser degree, for the lower WDM particle mass models. Our results for these particle mass models indicate that the luminosity density reaches an approximately constant level at the faint end, and thus the ionizing flux will remain constant at fainter luminosities. Deep observations with JWST certainly will much better determine the faint end slope α of the luminosity function. The reionization history is highly sensitive to this parameter. A future analysis could possibly circumvent the uncertainty stemming from fitting the evolution of the Schechter parameters, instead relying on direct observations of α for most redshifts.

We have neglected any evolution in the escape fraction with redshift. Naïvely, one might expect the escape fraction to decrease with redshift since the overall density scales as $(1+z)^3$. However, observations seem to indicate the opposite: the escape fraction increases with redshift. Mitra et al. (2012) found that $f_{\rm esc} \sim 0.06$ at $z \sim 6$, and increases to at least $f_{\rm esc} \gtrsim 0.146$ by $z \sim 10$. This could be caused by an initial mass function for star formation favoring high mass stars in the early universe. Alternatively, Ferrara & Loeb (2012) proposes a mechanism where mini haloes close to the cooling limit contributes appreciably to the ionizing flux, but their contribution diminishes over time due to feedback mechanisms. Since these small haloes have a relatively larger escape fraction the overall escape fraction decreases with time. This mechanism is especially interesting from a WDM perspective, since the lower abundance of small haloes directly counteracts this. The evolution of the escape fraction remains uncertain, and a typical constant value in previous work was $f_{\rm esc} \sim 20\%$, and our conservative choice of $f_{\rm esc} > 0.5$ will very unlikely overestimate the ionizing flux.

Non-stellar processes can potentially contribute to the reionization history. Quasars might play an important role at high redshift, although current results seem to indicate the contribution from quasars is sub-dominant (Volonteri & Gnedin 2009). For example, Willott et al. (2009) found that at $z \sim 6$ the ionizing flux from quasars is 20-100 times lower than the what is needed for continued reionization. X-ray emission by black holes may also contribute appreciably. Ricotti & Ostriker (2004) and Ricotti et al. (2005) analysed a pre-ionization contribution from a top-heavy ini-

tial mass function for the population III stars. These population III stars then collapse into black holes and subsequently accrete at nearly the Eddington limit. Accretion onto the black holes could partially reionize the IGM, although the primary effect would be heating the IGM. The population III phase is rapidly self-limiting due to pollution by heavy elements and pair instability supernovae causing strong outflows, and thus the metal-poor population III stars needs to collapse into black holes. This pre-ionization phase is then followed by a period of stellar reionization.

Bovill & Ricotti (2011) and Katz & Ricotti (2012) present a mechanism where the bulk of the star formation in the first dwarf galaxies happened in proto-globular clusters that were subsequently tidally stripped from the dwarf galaxy. Since the tidal stripping of globular clusters in the halo outskirts precede the stripping of the dark matter halo this can break the assumption of the abundance matching technique since the dwarf galaxies would be stripped of much of their luminous matter. Consequently, the mass-luminosity mapping would no longer be strictly monotonic, and the scatter on any mass-luminosity relation would likely increase. Importantly, for mass scales larger than the masses of these dark dwarf galaxies, however, the abundance matching would still give a meaningful average mass-luminosity mapping. In any case, the abundance matching we employ here would be an upper bound on the luminosity of a dwarf galaxy and, therefore, our approach is highly conservative.

In the case of sterile neutrino WDM, it has been shown that the effects of the radiative decay of sterile neutrino WDM to X-ray photons may catalyze the formation of H_2 and star formation (Biermann & Kusenko 2006). This does not affect the results presented here, because in this case the sterile neutrino WDM cosmology is constrained to produce the same observed high-z luminosity functions from which the reionization history is inferred. The only method by which such radiative decays would enhance the reionization rate is if they preferentially enhanced star formation for small mass halos below the luminosity function cutoff magnitude. We are aware of no mechanism in the literature that would produce such an enhancement for low mass halos. Moreover, this X-ray photon catalizatoin process would enhance star formation preferentially in metal free low mass halos that rely on H_2 to cool. More massive halos which are involved in reionizatoin are insensitive to this mechanism as they can cool by Lyα line emission and are more likely to be metal rich. Therefore, since halo formation is suppressed at these low masses, we believe our results apply for the case of sterile neutrino WDM, with the 3 keV and 6 keV mass scales disfavored at $> 10\sigma$ and 98.6% C.L., respectively.

Recall that the 1.3 keV (thermal; 6 keV sterile) model we have considered corresponds to model discussed by Lovell et al. (2012) as a solution to the too-big-to-fail problem (Boylan-Kolchin et al. 2012) and the M2L25 model studied in Boyarsky et al. (2009). We have demonstrated that this model is disfavored at 98.6% C.L. by direct galaxy counts at high redshift and is unable to reproduce the CMB optical depth even with extreme assumptions about the escape fraction.

6 CONCLUSION

We have shown that the Lyman-break technique for galaxy surveys at high redshift can provide a direct method for constraining the nature of dark matter and its clustering at small scales, with sensitivity to the structure formation suppression present in WDM models. We have analyzed CDM and WDM cosmological simulations in order to test WDM models using the luminosity function observations at high-z as well as a new analysis of cosmological reionization limits. Given the assumptions that the luminosity function of a ΛCDM universe is modeled by a Schechter function down to faint magnitudes and that the mass-luminosity relation of galaxies is independent of the dark matter model employed, we have modeled the luminosity function for several dark matter models to analyze the sensitivities to WDM dark matter models.

Using an approximate χ^2 test of the faint end of the luminosity function, direct number counts of galaxies significantly disfavors a 0.8 keV WDM model at greater than 10σ, and a 1.3 keV model is disfavored at approximately 98.6% C.L. (2.2σ). Further, with highly optimistic values for the parameters that translate high redshift galaxy luminosity to ionizing flux, the 0.8 keV and 1.3 keV model are inconsistent with the CMB optical depth at greater than 68% C.L. Furthermore, for the conservative case of a limiting luminosity of $M_{AB} = -13$, a 2.6 keV WDM model is only marginally consistent with the 68% confidence region of the optical depth from *Planck*. Wherever possible, we have used conservative values on parameters, making WDM behave more like cold dark matter. For this reason we feel confident concluding that neither the 0.8 keV or 1.3 keV models are consistent at more than 68% C.L. with reionization, even with the large uncertainty on the reionization process.

We expect upcoming deep surveys with JWST (and possibly HST via the Frontier Fields) to be able to reach luminosities and redshifts that can fully discern between a CDM model and a 1.3 keV model by direct number counts. Even 2.6 keV WDM might prove discernible if the observations are deep enough. Additionally, if the constraints on reionization parameters are improved, a 2.6 keV WDM model can be distinguished from cold dark matter by its different reionization history. The study of galaxy formation and reionization in the high-z universe adds a complementary and competitive probe to the nature of dark matter.

ACKNOWLEDGMENTS

We thank useful discussions with John Beacom and Richard Ellis. We would also like to thank the referee Massimo Ricotti for helpful feedback on the paper. KNA is partially supported by NSF CAREER Grant No. PHY-11-59224. JO and JSB were supported by grants from the NSF and NASA.

APPENDIX A: ABUNDANCE MATCHING WITH WARM DARK MATTER

Herpich et al. (2013) found that the star formation in low-z Milky-Way-like galaxies is slightly suppressed in WDM cosmologies. This seems to fit well with what one would expect: the small-scale cut-off in the WDM transfer function postpones the formation of dwarf galaxy halos, and therefore the potential wells that act as seeds for the first galaxies are shallower. The effect is relatively small, only a factor of 2 for their most extreme WDM model at $z = 0$.

The star formation efficiency for different dark matter models can readily be inferred from abundance matching. Figure A1 shows the halo mass-luminosity relation by using the different dark matter halo catalogues. For a fixed mass, a WDM halo is seen to be more luminous than a CDM halo, and thus WDM would, unsurprisingly, need to have an enhanced star formation efficiency

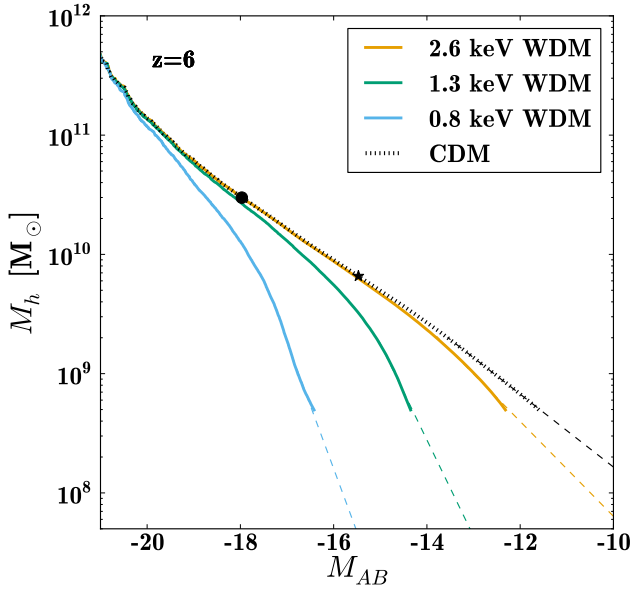

Figure A1. Abundance matching utilising the different halo catalogues. Abundance matching with the CDM catalogue gives a power law down to faint magnitudes. The dashed lines are power law extrapolations to the faint end. Clearly, the faint end in the WDM models diverge from the CDM power law towards more efficient star formation: lower mass halos have a larger luminosity relative to CDM. However, the WDM models must have roughly the same or a sligtly lower star formation rate than CDM, hence our assumption of the CDM power law behaviour is a very conservative estimate. The circle indicate the current HUDF magnitude limit, the asterisk is the expected JWST limits.

relative to CDM in order to match observations. This is counter-intuitive, and more importantly contradicts the low-z results of Herpich et al. (2013). A realistic WDM halo mass-luminosity mapping would give a slightly lower star formation efficiency: that is, a flatter slope than CDM in figure A1 instead of a steeper slope. In our analysis we therefore conservatively assume that the halo mass-luminosity is a power law. Therefore, a halo mass can uniquely be mapped to the same luminosity independent of WDM model.

REFERENCES

Abazajian K., 2006, Phys.Rev., D73, 063506, astro-ph/0511630

Abazajian K., Calabrese E., Cooray A., De Bernardis F., Dodelson S., et al., 2011, Astropart.Phys., 35, 177, 1103.5083

Ade P. A. R., Aghanim N., Armitage-Caplan C., Arnaud M., Ashdown M., Atrio-Barandela F., Aumont J., Baccigalupi C., Banday A. J., et al. 2013, ArXiv e-prints, 1303.5076, ADS

Angulo R. E., Hahn O., Abel T., 2013, 1304.2406

Barkana R., Haiman Z., Ostriker J. P., 2001, Astrophys.J., 558, 482, arXiv:astro-ph/0102304, ADS

Behroozi P. S., Wechsler R. H., Lu Y., Hahn O., Busha M. T., Klypin A., Primack J. R., 2013, ArXiv e-prints, 1310.2239, ADS

Biermann P. L., Kusenko A., 2006, Phys.Rev.Lett., 96, 091301, astro-ph/0601004

Bode P., Ostriker J. P., Turok N., 2001, ApJ, 556, 93, astro-ph/0010389

Bouwens R., Illingworth G., Oesch P., Trenti M., Labbe I., et al., 2011, 1105.2038

Bouwens R. J., Illingworth G. D., Franx M., Ford H., 2007, The Astrophysical Journal, 670, 928, 0707.2080

Bovill M. S., Ricotti M., 2011, Astrophys.J., 741, 18, 1010.2233

Boyarsky A., Lesgourgues J., Ruchayskiy O., Viel M., 2009, Phys.Rev.Lett., 102, 201304, 0812.3256

Boylan-Kolchin M., Bullock J. S., Kaplinghat M., 2012, Mon.Not.Roy.Astron.Soc., 422, 1203, 1111.2048

Bryan G. L., Norman M. L., 1998, Astrophys.J., 495, 80, arXiv:astro-ph/9710107, ADS

Calvi V., Pizzella A., Stiavelli M., Morelli L., Corsini E., et al., 2013, 1304.6093

Conroy C., Wechsler R. H., Kravtsov A. V., 2006, Astrophys.J., 647, 201, astro-ph/0512234

de Souza R. S., Mesinger A., Ferrara A., Haiman Z., Perna R., et al., 2013, MNRAS, 432,, 3218, 1303.5060

Dodelson S., Widrow L. M., 1994, Phys. Rev. Lett., 72, 17, hep-ph/9303287

Ellis R. S., McLure R. J., Dunlop J. S., Robertson B. E., Ono Y., Schenker M. A., Koekemoer A., Bowler R. A. A., Ouchi M., Rogers A. B., Curtis-Lake E., Schneider E., Charlot S., Stark D. P., Furlanetto S. R., Cirasuolo M., 2013, The Astrophysical Journal Letters, 763, L7, 1211.6804, ADS

Fan X., Strauss M. A., Becker R. H., White R. L., Gunn J. E., Knapp G. R., Richards G. T., Schneider D. P., Brinkmann J., Fukugita M., 2006, AJ, 132, 117, arXiv:astro-ph/0512082, ADS

Ferrara A., Loeb A., 2012, 1209.2123

Finlator K., Oh S. P., Ozel F., Dave R., 2012, 1209.2489

Garrison-Kimmel S., Boylan-Kolchin M., Bullock J., Lee K., 2013, ArXiv e-prints, 1310.6746, ADS

Hahn O., Abel T., 2011, Monthly Notices of the Royal Astronomical Society, 415, 2101, 1103.6031, ADS

Herpich J., Stinson G. S., Macciò A. V., Brook C., Wadsley J., Couchman H. M. P., Quinn T., 2013, ArXiv e-prints, 1308.1088, ADS

Horiuchi S., Humphrey P. J., Onorbe J., Abazajian K. N., Kaplinghat M., Garrison-Kimmel S., 2013, ArXiv e-prints, 1311.0282, ADS

Howlett C., Lewis A., Hall A., Challinor A., 2012, Journal of Cosmology and Astroparticle Physics, 4, 27, 1201.3654, ADS

Hu W., Kravtsov A. V., 2003, Astrophys.J., 584, 702, astro-ph/0203169

Jenkins A., 2010, Monthly Notices of the Royal Astronomical Society, 403, 1859, 0910.0258, ADS

Kamionkowski M., Liddle A. R., 2000, Phys. Rev. Lett., 84, 4525, arXiv:astro-ph/9911103, ADS

Katz H., Ricotti M., 2012, 1211.6153

Kistler M. D., Yuksel H., Beacom J. F., Hopkins A. M., Wyithe J. S. B., 2009, Astrophys.J., 705, L104, 0906.0590

Knebe A., Wagner C., Knollmann S., Diekershoff T., Krause F., 2009, The Astrophysical Journal, 698, 266, 0904.0083, ADS

Knollmann S. R., Knebe A., 2009, The Astrophysical Journal Supplement, 182, 608, 0904.3662, ADS

Kravtsov A. V., Berlind A. A., Wechsler R. H., Klypin A. A., Gottlöber S., Allgood B., Primack J. R., 2004, The Astrophysical Journal, 609, 35, arXiv:astro-ph/0308519, ADS

Kuhlen M., Faucher-Giguere C., 2012, 1201.0757

Kusenko A., 2006, Phys.Rev.Lett., 97, 241301, hep-ph/0609081

Lewis A., Challinor A., Lasenby A., 2000, The Astrophysical Journal, 538, 473, arXiv:astro-ph/9911177, ADS

Lovell M. R., Eke V., Frenk C. S., Gao L., Jenkins A., et al., 2012, Mon.Not.Roy.Astron.Soc., 420, 2318, 1104.2929

Lovell M. R., Frenk C. S., Eke V. R., Jenkins A., Gao L., et al.,

2013, 1308.1399
Lukić Z., Heitmann K., Habib S., Bashinsky S., Ricker P. M., 2007, The Astrophysical Journal, 671, 1160, arXiv:astro-ph/0702360, ADS
McLure R. J., Dunlop J. S., Bowler R. A. A., Curtis-Lake E., Schenker M., Ellis R. S., Robertson B. E., Koekemoer A. M., Rogers A. B., Ono Y., Ouchi M., Charlot S., Wild V., Stark D. P., Furlanetto S. R., Cirasuolo M., Targett T. A., 2012, p. 25, 1212.5222
Marsh D. J. E., Silk J., 2013, 1307.1705
Mitra S., Ferrara A., Choudhury T. R., 2012, 1207.3803
Moster B. P., Naab T., White S. D. M., 2013, MNRAS, 428, 3121, 1205.5807, ADS
Oesch P., Bouwens R., Illingworth G., Labbe I., Franx M., et al., 2013, 1301.6162
Oesch P. A., Bouwens R. J., Illingworth G. D., Labbe I., Franx M., van Dokkum P. G., Trenti M., Stiavelli M., Gonzalez V., Magee D., 2013, p. 21, 1301.6162
Pacucci F., Mesinger A., Haiman Z., 2013, 1306.0009
Polisensky E., Ricotti M., 2011, Phys.Rev., D83, 043506, 1004.1459
Polisensky E., Ricotti M., 2013, ArXiv e-prints, 1310.0430, ADS
Prunet S., Pichon C., Aubert D., Pogosyan D., Teyssier R., Gottloeber S., 2008, The Astrophysical Journals, 178, 179, 0804.3536, ADS
Reed D. S., Smith R. E., Potter D., Schneider A., Stadel J., Moore B., 2013, Monthly Notices of the Royal Astronomical Society, 431, 1866, 1206.5302, ADS
Ricotti M., Ostriker J. P., 2004, Mon.Not.Roy.Astron.Soc., 352, 547, astro-ph/0311003
Ricotti M., Ostriker J. P., Gnedin N. Y., 2005, Mon.Not.Roy.Astron.Soc., 357, 207, astro-ph/0404318
Robertson B. E., Furlanetto S. R., Schneider E., Charlot S., Ellis R. S., et al., 2013, 1301.1228
Schenker M. A., Robertson B. E., Ellis R. S., Ono Y., McLure R. J., et al., 2013, Astrophys.J., 768, 196, 1212.4819
Schneider A., Smith R. E., Reed D., 2013, 1303.0839
Shaposhnikov M., Tkachev I., 2006, Phys.Lett., B639, 414, hep-ph/0604236
Shi X.-d., Fuller G. M., 1999, Phys. Rev. Lett., 82, 2832, astro-ph/9810076
Sobacchi E., Mesinger A., 2013, 1301.6781
Somerville R. S., Bullock J. S., Livio M., 2003, The Astrophysical Journal, 593, 616, arXiv:astro-ph/0303481, ADS
Springel V., 2005, Mon.Not.Roy.Astron.Soc., 364, 1105, astro-ph/0505010
Trujillo-Gomez S., Klypin A., Primack J., Romanowsky A. J., 2011, Astrophys.J., 742, 16, 1005.1289
Vale A., Ostriker J., 2004, Mon.Not.Roy.Astron.Soc., 353, 189, astro-ph/0402500
Viel M., Becker G., Bolton J., Haehnelt M., 2013, 1306.2314
Viel M., Lesgourgues J., Haehnelt M. G., Matarrese S., Riotto A., 2005, Phys.Rev., D71, 063534, astro-ph/0501562
Villaescusa-Navarro F., Dalal N., 2011, JCAP, 1103, 024, 1010.3008
Volonteri M., Gnedin N., 2009, Astrophys.J., 703, 2113, 0905.0144
Wang J., White S. D., 2007, Mon.Not.Roy.Astron.Soc., 380, 93, astro-ph/0702575
Willott C. J., Delorme P., Reyle C., Albert L., Bergeron J., et al., 2009, 0912.0281
Windhorst R. A., Cohen S. H., Jansen R. A., Conselice C., Yan H.-J., 2006, New Astron.Rev., 50, 113, astro-ph/0506253
Zahn O., Reichardt C., Shaw L., Lidz A., Aird K., et al., 2012, Astrophys.J., 756, 65, 1111.6386
Zentner A. R., Bullock J. S., 2002, Phys.Rev., D66, 043003, arXiv:astro-ph/0205216, ADS